Synthetic and Systems Biotechnology 8 (2023) 498–508

Contents lists available at ScienceDirect

Synthetic and Systems Biotechnology

journal homepage: www.keaipublishing.com/en/journals/synthetic-and-systems-biotechnology

Original Research Article

Construction and application of high-quality genome-scale metabolic model of *Zymomonas mobilis* to guide rational design of microbial cell factories

Yalun Wu [a,1], Qianqian Yuan [b,1], Yongfu Yang [c,d,a,1], Defei Liu [b], Shihui Yang [a,*], Hongwu Ma [b,**]

[a] State Key Laboratory of Biocatalysis and Enzyme Engineering, School of Life Sciences, Hubei University, Wuhan, 430062, Hubei, China
[b] Biodesign Center, Key Laboratory of Systems Microbial Biotechnology, Tianjin Institute of Industrial Biotechnology, Chinese Academy of Sciences, Tianjin, 300308, China
[c] Hubei Key Laboratory of Applied Mathematics, Faculty of Mathematics and Statistics, Hubei University, Wuhan, 430062, Hubei, China
[d] Artificial Intelligence and Knowledge Engineering Lab, School of Computer Science and Information Engineering, Hubei University, Wuhan, 430062, Hubei, China

ARTICLE INFO

Keywords:
Genome-scale metabolic models (GEMSs)
Non-model industrial microorganism
Zymomonas mobilis
Biolog phenotype microarray
Succinate
1,4-Butanediol

ABSTRACT

High-quality genome-scale metabolic models (GEMs) could play critical roles on rational design of microbial cell factories in the classical Design-Build-Test-Learn cycle of synthetic biology studies. Despite of the constant establishment and update of GEMs for model microorganisms such as *Escherichia coli* and *Saccharomyces cerevisiae*, high-quality GEMs for non-model industrial microorganisms are still scarce. *Zymomonas mobilis* subsp. *mobilis* ZM4 is a non-model ethanologenic microorganism with many excellent industrial characteristics that has been developing as microbial cell factories for biochemical production. Although five GEMs of *Z. mobilis* have been constructed, these models are either generating ATP incorrectly, or lacking information of plasmid genes, or not providing standard format file. In this study, a high-quality GEM *i*ZM516 of *Z. mobilis* ZM4 was constructed. The information from the improved genome annotation, literature, datasets of Biolog Phenotype Microarray studies, and recently updated Gene-Protein-Reaction information was combined for the curation of *i*ZM516. Finally, 516 genes, 1389 reactions, 1437 metabolites, and 3 cell compartments are included in *i*ZM516, which also had the highest MEMOTE score of 91% among all published GEMs of *Z. mobilis.* Cell growth was then predicted by *i*ZM516, which had 79.4% agreement with the experimental results of the substrate utilization. In addition, the potential endogenous succinate synthesis pathway of *Z. mobilis* ZM4 was proposed through simulation and analysis using *i*ZM516. Furthermore, metabolic engineering strategies to produce succinate and 1,4-butanediol (1,4-BDO) were designed and then simulated under anaerobic condition using *i*ZM516. The results indicated that 1.68 mol/mol succinate and 1.07 mol/mol 1,4-BDO can be achieved through combinational metabolic engineering strategies, which was comparable to that of the model species *E. coli.* Our study thus not only established a high-quality GEM *i*ZM516 to help understand and design microbial cell factories for economic biochemical production using *Z. mobilis* as the chassis, but also provided guidance on building accurate GEMs for other non-model industrial microorganisms.

1. Introduction

Robust and efficient microbial cell factories are crucial for biomanufacturing and the transformation of petroleum-based economy to sustainable bioeconomy [1]. The rational design of cell factories is becoming reality with the development of systems and synthetic biology. Before the practices of metabolic engineering, it is important to investigate the metabolic network within the chassis cells to identify

Peer review under responsibility of KeAi Communications Co., Ltd.
* Corresponding author.
** Corresponding author.
E-mail addresses: aaronwu@stu.hubu.edu.cn (Y. Wu), yuan_qq@tib.cas.cn (Q. Yuan), yongfu.yang@stu.hubu.edu.cn (Y. Yang), liudf@tib.cas.cn (D. Liu), Shihui.Yang@hubu.edu.cn (S. Yang), ma_hw@tib.cas.cn (H. Ma).
[1] Equal contribution.

https://doi.org/10.1016/j.synbio.2023.07.001
Received 21 February 2023; Received in revised form 4 July 2023; Accepted 4 July 2023
Available online 6 July 2023

metabolic pathways and genetic targets associated with them for genetic manipulation. Genome-scale metabolic model (GEM) is an effective tool to simulate metabolic fluxes *in silico* with algorithms such as flux balance analysis (FBA) [2]. Meanwhile, GEM can be used to perform metabolic analyses under different conditions, explore new scientific findings, and guide the design and modification of metabolic pathways and synthetic microorganisms for economic biochemical production [3].

High-quality GEMs have been constantly established and updated for model microorganisms such as *E. coli* [2] and *S. cerevisiae* [4]. For example, the model *i*JE660 was the first GEM of *E. coli* after its genome was sequenced [5]. After that, a series of GEMs were reconstructed with different degrees of quality improvement [2]. *i*ML1515 was the latest stoichiometric model of *E. coli*, of which ~50% of function-known genes (1515 genes) were included in the model [6]. Meanwhile, *i*ML1515 integrated with 1515 protein structural information, enabling analysis of structural proteome comparison and evaluation of mutational impact across strains [6]. Recently, multiple constraints of thermodynamic and enzymatic were integrated into *i*ML1515, making the pathway analysis and phenotype prediction more realistic [7]. The same development route happened with the yeast model [4], into which the enzyme constraints were introduced recently [8].

However, similar work is still scarce for non-model microorganisms with excellent characteristics from industrial practices. *Zymomonas mobilis* is a gram-negative ethanologenic bacterium with unique physiological properties and extraordinary ethanol production characteristics such as high sugar uptake rate, high ethanol yield and ethanol tolerance [9], which is the only known microorganism that can utilize the Entner-Doudoroff (ED) pathway under anaerobic conditions [10]. Therefore, *Z. mobilis* has been engineered for economic production of a variety of biofuels and biochemicals such as lignocellulosic ethanol [11,12], poly-3-hydroxybutyrate (PHB) [13], D-lactic acid [14,15], 2,3-butanediol [16], sorbitol [17], acetaldehyde [18], and isobutanol [19].

Although five GEMs of *Z. mobilis* have been published, no standard format files were provided before 2020 with only the reaction sets involved in the model attached, which cannot be directly reused for simulation [20,21]. Recently, two models *i*HN446 and *i*ZM4_478 were published with standard SBML files, but still suffered from issues. For example, amino acids are needed to support cell growth for the *i*HN446 model, although previous results exhibited that *Z. mobilis* is not an amino acid deficient strain and amino acids are not necessary for its growth in minimal medium [22], which suggests that wrong pathway(s) may be included in model *i*HN446 [23]. Meanwhile, instead of 1 mol ATP per 1 mol glucose under anaerobic condition, *i*HN446 produced incorrect amount of 3 mol ATP per 1 mol glucose. Furthermore, most published GEMs of *Z. mobilis* ZM4 lack plasmid gene information. The genome of *Z. mobilis* ZM4 was sequenced and released in 2005, which contained a circular chromosome with 1998 open reading frames (ORF) [24]. In 2009, the genome annotation of ZM4 was improved by combining systems biology approaches of genome resequencing and proteomics study [25]. The accurate genome sequence of *Z. mobilis* containing gene information of a revised chromosome and four native plasmids was further updated in 2018 [26], which could help revisit and improve the GEM of *Z. mobilis*. However, only iHN446 included four plasmid genes, and other models did not contain any plasmid information.

In contrast, the *i*ZM516 constructed in this study for *Z. mobilis* ZM4 combined the information of the improved genomic annotation including plasmid, datasets of Biolog Phenotype Microarrays experiments, literature, and Gene-Protein-Reaction information of the recent models. Meanwhile, we further solved the mass balance and ATP infinite generation problems to ensure the quality of model, and used the standard genome-scale metabolic model test suite MEMOTE to improve the model quality. The construction of high-quality *i*ZM516 model can then be applied to help design the effective metabolic pathways for the production of succinate and 1,4-butanediol in *Z. mobilis*.

2. Materials and methods

2.1. Construction of the draft model using ModelSEED

The latest genomic information of *Z. mobilis* subsp. *mobilis* ZM4 (chromosome: NZ_CP023715.1/CP023715.1, plasmid pZM32: NZ_CP023716.1/CP023716.1, plasmid pZM33: NZ_CP023717.1/CP023717.1, plasmid pZM36: NZ_CP023718.1/CP023718.1, and plasmid pZM39: NZ_CP023719.1/CP023719.1) was used for model construction, and the online webserver Rapid Annotation using Subsystem Technology (RAST) was used to annotate genome with option "Build metabolic model", which will automatically build draft model with ModelSEED [27]. The temporary gene IDs annotated by RAST were transformed into specific IDs and names of *Z. mobilis* ZM4 by BLASTp with the latest *Z. mobilis* genome annotation from NCBI as reference [28]. In this process, the threshold of homologues was set as e-value $\leq 10^{-5}$, and the identity $\geq$40%. In addition, the information of genes, reactions, and metabolites of the draft model was improved by integrating the information from MetaCyc [29], Biochemical, Genetic and Genomic (BiGG) knowledge base [30], Kyoto Encyclopedia of Genes and Genomes (KEGG), BRaunschweig ENzyme DAtabase (BRENDA) [31], and other databases [32].

2.2. Biomass synthesis curation and automatic gap filling

Biomass composition usually includes DNA, RNA, proteins, lipids, peptidoglycan, carbohydrates, and small molecules. In this study, biomass composition was set referred to the published literature [20,21], and was made up of 15 sub-reactions. Macromolecules are important in the biomass synthesis. When there is a synthetic or a putative synthetic pathway for a macromolecule, relevant reactions are involved in the model, such as the biosynthesis of fatty acids and hopanes in *Z. mobilis* [33]. Hopane is an important membrane component of *Z. mobilis* contributing to ethanol tolerance, and the possible metabolic pathway of hopane was reported in literature [33]. Combining the hopane biosynthesis pathway PWYN-7072 from the MetaCyc database and the literature, the hopane biosynthesis module was cured in *i*ZM516 constructed in this study. If the detailed knowledge of some macromolecule synthesis was not very clear, a total reaction equation was used for these macromolecules, and the sub-reactions were ignored.

Metabolic gaps usually occur in the draft model, resulting in the inability of model to synthesize biomass. To achieve automatic gap filling, a weight-added pFBA algorithm was used [34]. Briefly, biomass compositions that cannot be synthesized in the model were identified firstly. Then, the gaps in each composition synthesis pathway were confirmed using FBA calculation. Finally, the weight-added pFBA gap-filling algorithm was employed to fill the gaps. The reactions in the draft model were all set weight as 1000, and the upper limit of the biomass equation was set as 0.1 to minimize the filling reaction numbers introduced from ModelSEED database [34]. In this way, the reactions in the draft model will be preferentially used in calculation. When there is a gap in the calculational pathway, the missing reactions are automatically retrieved from the reactions of ModelSEED database. To ensure the correction of added reactions and determine the Gene-Protein-Reaction (GPR) relations, manual checks were performed if necessary.

2.3. ATP synthesis and respiratory chain correction

Except for a few well-known ATP generation reactions, general principles were used for ATP generation correction including [35]: 1) The reaction of ATP to AMP conversion is irreversible. 2) If the reaction generating ATP from ADP does not possess carbon-containing metabolites, the direction is set to consume ATP except for the known ATP synthesis reactions. 3) Reaction with oxygen generation is generally irreversible. 4) Transamination is usually the decomposition reaction of amino acids. 5) If the reaction does not involve in above principles,

manual check is performed combined with MetaCyc, KEGG, and eQuilibrator [32] databases.

2.4. Biolog Phenotype Microarray experiments and data analysis

The Biolog Phenotype Microarrays (PMs) were employed to test the substrates utilization of different carbon, nitrogen, sulfur, and phosphorus sources with the Omnilog PM automatic system using the wild-type strain *Z. mobilis* ZM4. It was reported that the phenotype of *Z. mobilis* was similar to that of yeast in the previous study [36]. Therefore, the experimental process was referred to the PMs Procedure for *S. cerevisiae* and other Yeast. The image data of PMs were processed into values using OmniLog PM program suite of data processing and analysis based on the operational manual. Then, the FBA calculation was performed with the biomass equation as the objective function, either the metabolites in PM1 and PM2 were set as the only carbon source, or the metabolites in PM3, PM4 A1-E12, or PM4 F1–H12 were set as the only nitrogen, sulfur, or phosphorus source, respectively.

2.5. Model simulation analysis, evaluation, and visualization

The GEM *i*ML1515 of *E. coli* was used to simulate chemical production in *E. coli* [6]. COBRApy is a Python-based toolkit package, which can be used to modify model, generate executable file, and simulate analyses such as FBA, Parsimonious flux balance analysis (pFBA), flux variability analysis (FVA), and gene necessity analysis [37]. The model was evaluated by MEMOTE to check the mass balance, charge balance, and model annotation [38]. All simulations were performed under anaerobic condition in minimal media with oxygen uptake rate set as 0, glucose as sole C sources with 40 mmol/gDW/h uptake rate, ammonia as sole N sources with 1000 mmol/gDW/h uptake rate unless otherwise indicated. When the cell growth was taken into consideration, the biomass growth rate was set as 0.1 h^{-1}.

3. Results

3.1. Construction of the GEM iZM516 and comparison of published models

In this study, a new genome-scale metabolic model for *Z. mobilis* ZM4 was constructed using modelSEED, and then model curation and verification were performed based on the experimental data and latest information. Finally, the new model was named as *i*ZM516 (**Supplementary file 1: SBML version file of *i*ZM516**), which contains 1389 reactions, 1437 metabolites, and 516 genes with 6 genes located on native plasmids corresponding to 80 reactions (Table S1). *i*ZM516 also contains 3 cell compartments of intracellular, periplasmic, and extracellular.

Z. mobilis uses ED pathway to ferment glucose under anaerobic condition, which results in only 1 mol of ATP yielded per mol glucose. Using the ATP maintenance (ATPM) reactions (atp_c + h2o_c → adp_c + h_c + pi_c) as objective function, three models (*i*ZM516, *i*ZM4_478 and *i*HN446) were compared with glucose uptake rate set as 10 mmol gDW^{-1} h^{-1}. 10 mmol gDW^{-1} h^{-1} ATP was generated using either *i*ZM516 or *i*ZM4_478 while 30 mmol gDW^{-1} h^{-1} ATP was generated using *i*HN446, which means *i*HN446 used incorrect pathway under anaerobic condition (Table 1). The pentose phosphate pathway (PPP) was incomplete in *Z. mobilis*, which lacks of 6-phosphogluconate (6 PG) dehydrogenase catalyzing 6 PG to form ribulose-5-phosphate (Ru5P) (6 pg_c + nad_c → ru5p_c + co2_c + nadh_c) [39,40]. However, *i*HN446 contains a reaction R10221 (6 pg_c + nad_c → ru5p_c + co2_c + nadh_c) with GPR annotation as ZMO0942, which is inaccurate and results in the PPP available in the model. Meanwhile, *i*HN446 uses ATP synthesis reaction (R00086: adp_c + 4.0 h_e + pi_c <=> atp_c + h2o_c + 3.0 h_c) to generate ATP under anaerobic condition, which contributes to the incorrection of simulation results of *i*HN446.

Table 1
Comparisons of ATP generation using different models with ATP maintain reaction as the objective function under aerobic or anaerobic conditions. The glucose uptake rate was set as 10 mmol $gDW^{-1}h^{-1}$.

	*i*ZM516	*i*ZM4_478	*i*HN446
Anaerobic	10	10	30
Aerobic	30	20	30

For aerobic condition, *Z. mobilis* uses a structural respiratory chain that mainly includes type II NADH dehydrogenase (Ndh, ZMO1113), coenzyme Q10, terminal oxidase cytochrome bd (CydAB, ZMO1571-ZMO1572), and other unidentified components [41]. Meanwhile, *Z. mobilis* is one of the few bacteria known to use NADH and NADPH as electron donors for the respiratory type II NADH dehydrogenase [42]. However, *i*ZM4_478 does not contain the reaction using NADPH as the electron donor. Glucose and lactate can also contribute electrons to the respiratory chain by donating electrons to the membrane-bound glucose dehydrogenase (Gdh, ZMO0558) and lactate dehydrogenase (Ldh, ZMO0256), respectively, which are transferred to coenzyme Q10 and subsequently to terminal oxidases that reduce oxygen to water [43]. In addition, because the respiratory chain of *Z. mobilis* may be completed in the periplasm [43], periplasm was introduced into the model as the third compartment with suffix "_p". Except for *i*ZM4_478, *i*HN446 and all other published models do not include periplasm compartment. Instead, the above genes and reactions involved in the respiratory chain are included in the current model *i*ZM516.

Since ATP generation under aerobic condition was associated with proton motive force (PMF), the reaction involved with h_p production and consumption in the model may affect ATP generation. However, there is no enough data to support the exact reactions that are associated with h_p in *Z. mobilis*. The comparison results of three models shown that *i*ZM516 and *i*HN446 generate 30 mmol gDW^{-1} h^{-1} ATP, and *i*ZM4_478 generates 20 mmol gDW^{-1} h^{-1} ATP (Table 1). This difference resulted from different h_p containing reactions involved in different models. In the simulation, *i*HN446 does not contain periplasm compartment, and must supply amino acids in the medium for cell growth, which is not the essential nutritional requirement for *Z. mobilis* [22]. Hence, *i*HN446 was not included for further simulation comparison.

Although the latest published model *i*ZM4_478 has improved GPR association through pooled transposon mutant fitness experiments [44], *i*ZM516 further corrected GPR association based on experiment results such as ^{13}C-labelled metabolomics data [39] and the latest literature, such as *ZMO1754* encoding an $NADP^+$-dependent acetaldehyde dehydrogenase that was determined recently [45]. All manual curation reaction list can be found in supplementary materials (**Supplementary file 2**). Compared with five published GEMs of *Z. mobilis*, *i*ZM516 has the largest datasets of genes, reactions, and metabolites (Table 2) containing 25.8% (516/2001) of totally annotated genes of ZM4. Based on the enrichment results, these 516 genes were mainly distributed in metabolism, transporter, and tRNA synthesis, while amino acid metabolism contains the largest gene number of 139 (Fig. S1). The number of genes in *i*ZM516 was also 8% larger than that in *i*ZM4_478 without genes from native plasmids. Based on the gene number comparisons, 380 genes were all included in *i*ZM516, *i*ZM4_478, and *i*HN446. However, there are 60 unique genes in *i*ZM516, 27 unique genes in *i*ZM4_478, and 28 unique genes in *i*HN446, respectively (Fig. S2). The reactions associated with these unique genes in *i*ZM4_478 or *i*HN446 are either already presented in *i*ZM516 but associated with other genes, or uncertain whether they exist but not affect biomass synthesis. Therefore, these genes were not introduced into *i*ZM516.

3.2. Biolog Phenotype Microarrays experiments and data correction

Biolog Phenotype Microarrays (PMs) experiments were employed to evaluate and confirm the metabolic capabilities of *Z. mobilis*. The

Table 2
Comparisons of genome-scale metabolic models of *Z. mobilis*.

Model	*i*ZM516	*i*ZM4_478	*i*HN446	*i*EM439	*i*ZM363	ZmoMBEL601
Strain	ZM4	ZM4	ZM4	ZM1	ZM4	ZM4
SBML file [a]	+	+	+	–	–	–
Compartment	3	3	2	2	2	2
Genes	516	478	446	439	363	348
Plasmid genes	6	0	4	0	0	0
Reactions	1389	857	859	692	747	601
Metabolites	1437	799	894	658	704	579
Year	2022	2020	2020	2016	2011	2010
Ref.	This study	[44]	[23]	[46]	[21]	[20]

[a] + SBML file available, - SBML file not available.

phenotype plates of carbon sources (PM1, PM2A), nitrogen sources (PM3B), phosphorus sources (PM4 A1-E12), and sulfur sources (PM4 F1–H12) were measured in the PM system to determine the utilization of different C, N, P, and S related substrates as the sole source. The 2 replicate of Biolog's PMs experiments data have high consistency with R^2 value of 0.96 (Fig. S3). For quantitative analysis, the max-height data of each well based on the average value of 2 replicates were used to compare with those of the control wells. If the value of test well was 1.5 times higher than that of the control well, the substrate was considered as responsive to *Z. mobilis*. The results showed that *Z. mobilis* responded to 91 substrates including 13 Carbon, 19 Nitrogen, 43 Phosphorus, and 16 Sulfur substrates (Table S2), which was consistent with the previous report [36]. All responsive substrates were simulated using the draft model as the sole carbon, nitrogen, or sulfur sources and some of which were included in *i*ZM516 by adding the corresponding transport reactions.

Wild-type *Z. mobilis* ZM4 can only utilize glucose, fructose, and sucrose as sole carbon sources, and cannot use pentoses such as xylose and arabinose. In both PM1 and PM2A plates, *Z. mobilis* not only responded to glucose and fructose, but also responded to xylose, arabinose, and other carbon sources weakly as shown in the kinetic curves (Fig. 1), which is consistent with a previous study [36]. In addition, sucrose (PM1_D11) in PM1 plate had no response, which is also consistent with a previous study that no response was observed even at high initial cell concentrations, and the previous study indicated that sucrose may subject to strong catabolite repression in the PM system [36]. The weak response to pentose carbon sources and no response to sucrose may be related to the mechanism of the PM system or unknown redox reaction

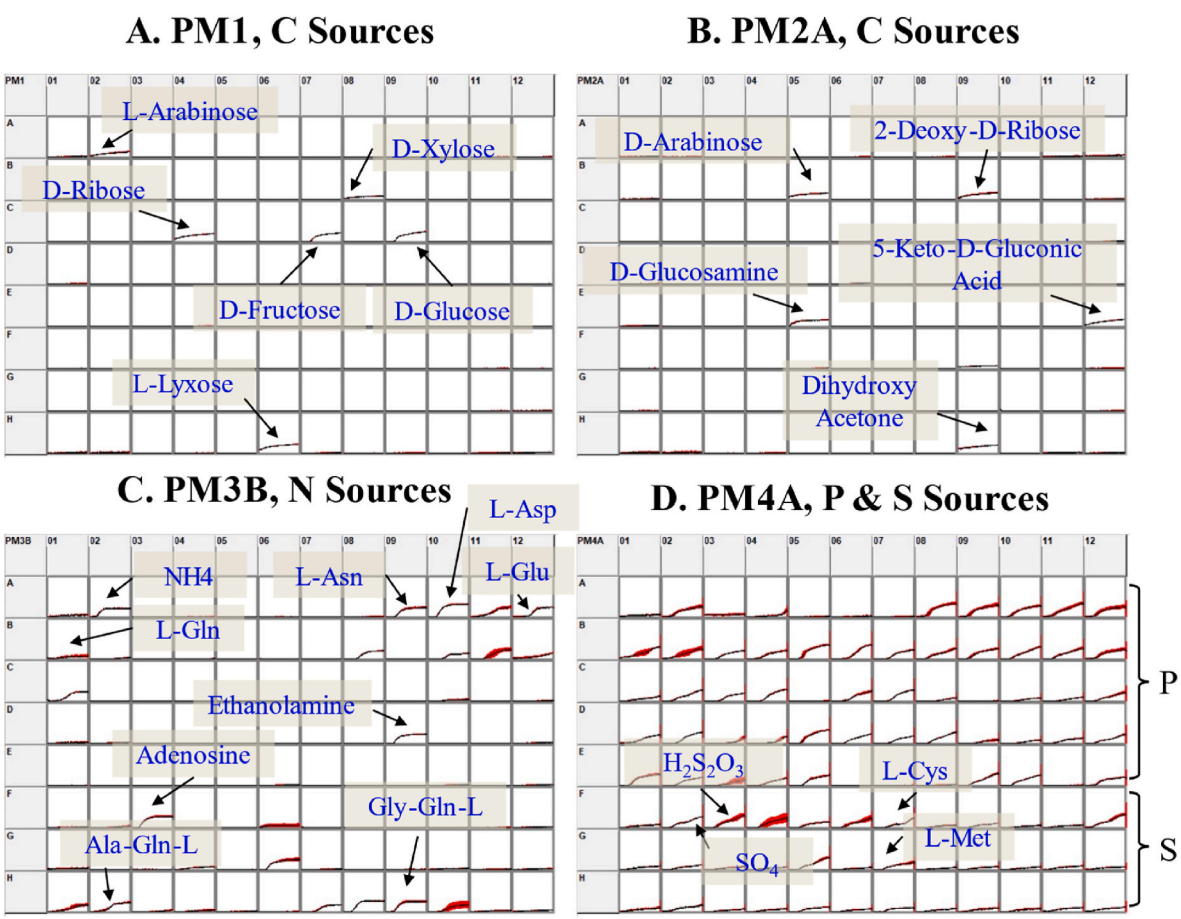

Fig. 1. Biolog Phenotype Microarrays profiling of *Z. mobilis* under different carbon (A, B), nitrogen (C), phosphorus and sulfur (D) sources. Each plate contains A-H rows and 01–12 columns, and the detail substrate information of each cell can be found in Table S2. L-Asn: L-Asparagine; L-Asp: L-Aspartic Acid; L-Cys: L-Cysteine; L-Glu: L-Glutamic Acid; L-Met: L-Methionine; Ala-Gln-L: L-Alanyl-glutamine; Gly-Gln-L: L-glycyl-glutamine. The blue font in the graph indicates the substrate in the cell.

of *Z. mobilis*.

It was reported that *Z. mobilis* can utilize NH_4^+, glutamic acid, glutamine, aspartate, and asparagine as nitrogen sources [36]. *i*ZM516 can utilize more than 10 different nitrogen sources including NH_4^+, asparagine, cysteine, glutamic acid, serine, ethanolamine, adenosine, and some peptides (Table S2). The result of PM4A phenotype plates (A1-E12) indicated that *Z. mobilis* can utilize 39 phosphorus sources except for pyrophosphate and tripolyphosphate (Fig. 1, Table S2), which is consistent with the previous study too [36]. *i*ZM516 simulation showed that 12 substrates can be used as the sole phosphorus source when used the sink reaction (Table S2). The result of PM4A phenotype plate (F1–H12) showed that 16 substrates can be the sole sulfur source (Fig. 1, Table S2). Shake flask experiments confirmed that sulfate, thiosulfate, cysteine, and methionine can be utilized as the sole sulfur source for *Z. mobilis* [47]. Correspondingly, the transport and exchange reactions were added to the model.

Furthermore, total 379 substrates were used to compare the different substrate utilization capabilities of *i*ZM516 and *i*ZM4_478. The results suggested that *i*ZM516 has an agreement of 79.4% (17 true positives and 284 true negatives) with experimental data, which is higher than that of 76.5% obtained by *i*ZM4_478, especially in true positive results (Fig. 2, Table S2). As for the remaining 74 false negative results with unknown encoding genes and pathways, no reactions were added into *i*ZM516 to predict growth. Optimization will be updated accordingly in the future studies.

3.3. Model evaluation by MEMOTE and cell growth validation

MEMOTE is a set of standardized metabolic model tests, which evaluates the metabolic model from multiple perspectives, and the resultant score could help identify the possible problems to improve the quality of the model [38]. Among the published models with simulation ready format files, only *i*ZM4_478 can be tested by MEMOTE, and *i*HN446 cannot be tested by MEMOTE with unknown reason. According to MEMOTE scoring (Fig. 3A and B), the standardized score of *i*ZM516 (91%, **Supplementary file 3**) was higher than that of *i*ZM4_478 (80%, **Supplementary file 4**). The accuracy of the mass and charge balance is better than 99% for both models, while only a few reactions in macromolecular synthesis were imbalanced. This demonstrated the comprehensiveness of *i*ZM516 for subsequent simulations.

As mentioned above, wild-type *Z. mobilis* can only utilize glucose, fructose, and sucrose. The growth rate of *Z. mobilis* in minimal medium (MM) is 0.13–0.45 h^{-1}, and the maximum uptake rate of glucose can be 60 $mmol{\cdot}gDW^{-1}{\cdot}h^{-1}$ [48]. When FBA was performed to evaluate the accuracy of *i*ZM516 and the glucose uptake rate was set from 0 to 70 $mmol{\cdot}gDW^{-1}{\cdot}h^{-1}$, the simulation results showed that the simulated specific growth and ethanol productivities of *i*ZM516 and *i*ZM4_478 were both consistent with experimental data (Fig. 3C and D) from literature reports [39,48,49]. The relevant analysis codes are provided in the **Supplementary file 5**.

3.4. Exploration of succinate biosynthesis pathway in Z. mobilis

Succinate is an important platform chemical for the synthesis of numerous chemical products, such as 1,4-butanediol, tetrahydrofuran, and bio-polyesters. It was experimentally confirmed that *Z. mobilis* can produce succinate under anaerobic condition [50,51], but the exact succinate synthetic pathway in wild-type *Z. mobilis* was not illustrated completely yet although the incomplete TCA cycle in *Z. mobilis* lacking two key genes encoding 2-oxoglutarate dehydrogenase complex (SucAB) and malate dehydrogenase (Mdh) could be used for succinate biosynthesis [40]. Previous research proposed that succinate was synthesized via the fumarate reduction reaction with the succinate precursor converted from pyruvate through malic enzyme (MaeA) (Fig. 4A) [20,50,52]. However, the [6–^{13}C] and [1–^{13}C] labelled fluxes analysis results exhibited that PEP was the predominant anaplerotic source of carbon for TCA [39], which suggested that succinate was not synthesized from pyruvate naturally in *Z. mobilis* (Fig. 4A). The ^{13}C labelled fluxes analysis also indicated that succinate was not produced from α-ketoglutarate via oxidative TCA cycle with the truncated TCA cycle, which suggested that there must exist substitutional pathway for succinate production in *Z. mobilis*.

Using the genome-scale model *i*ZM516, *in silico* analysis was performed to simulate anaerobic succinate production in *Z. mobilis*. Taking both the biomass synthesis and succinate production into consideration, the glucose uptake rate was set as 40 mmol/gDW/h, the biomass growth rate was set as 0.1 h^{-1}, then the maximization of succinate production was set as the objective function. The pFBA result suggested that succinate production in *Z. mobilis* may go through a complicated pathway (Fig. 4A). The flux starts from phosphoenolpyruvate (Pep) to oxaloacetate (Oaa) by a phosphoenolpyruvate carboxylase (ZMO1_ZMO1496, Ppc), which is then converted to aspartate (Asp) through an aminotransferase. Subsequently, Asp is catalyzed to fumarate (Fum) by different routes, which is finally reduced to succinate (Succ) through dihydroorotate dehydrogenase (ZMO1_ZMO0120) (Fig. 4A). Due to the complicated network for succinate generation, the simulation yield of succinate was pretty low at 0.03 mol Succ/mol glucose (0.017 g/g glucose) in wild-type *Z. mobilis* with ethanol or lactate as the primary products. This result is partially consistent with the ^{13}C fluxes analysis result that aspartate was produced from PEP and then to succinate [39]. However, simulation using *i*ZM4_478, succinate was produced from Akg through the reaction of OXGDC (akg_c + h_c <=> co2_c + sucsal_c) with GPR correlation gene of *ZMO0687*, which does not catalyze this reaction with the annotation of acetolactate synthase large subunit. Thus, the

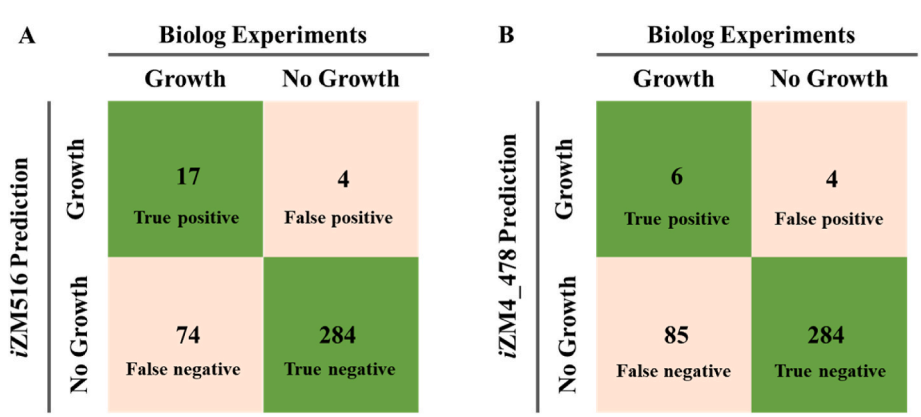

Fig. 2. Comparisons of *in silico* simulation and Biolog Phenotype Microarrays results of *i*ZM516 (A) and *i*ZM4_478 (B) for the utilization of various substrates. True positive and true negative means that the *in silico* simulation results were same as the *in vivo* experiments, while false positive means the substrate can be used in simulation but cannot be used *in vivo*. False negative is in contrast with false positive.

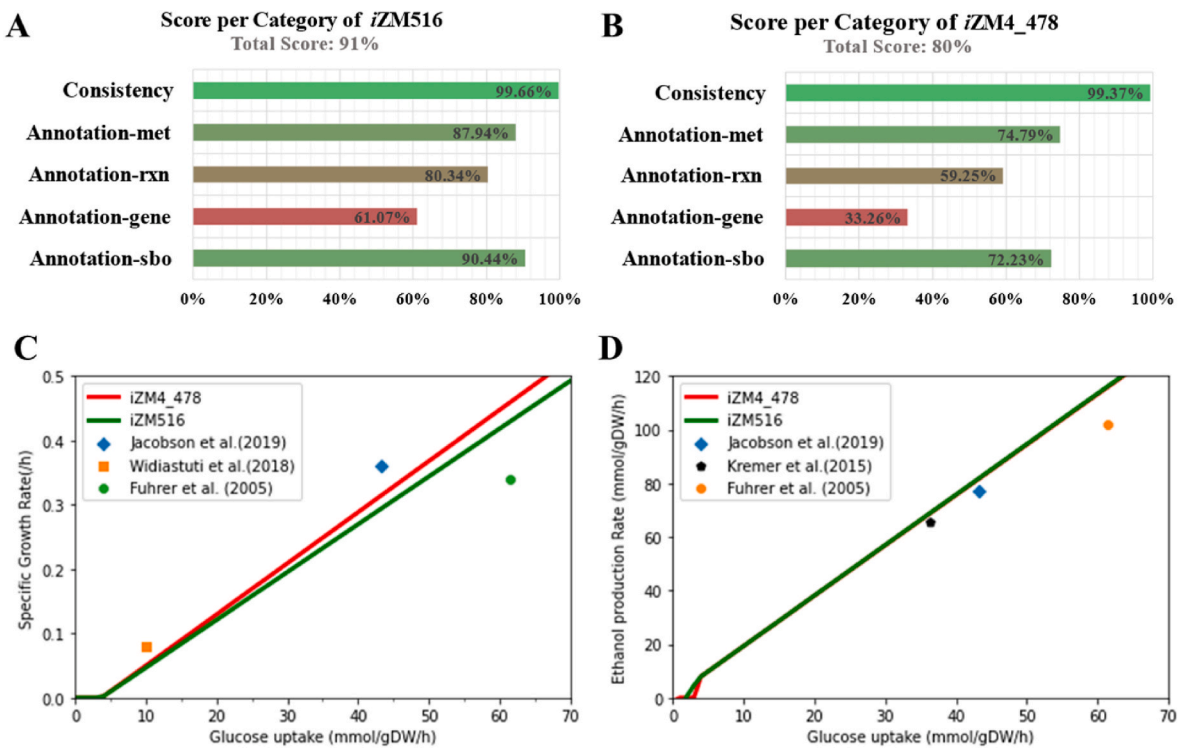

Fig. 3. Comparisons of MEMOTE test scores of *i*ZM516 (A) and *i*ZM4_478 (B) as well as the predictions for specific cell growth rates (C), and ethanol production fluxes (D) under anaerobic condition using *i*ZM516 (green line) or *i*ZM4_478 (red line) models. iZM4_478 is a model published recently. iZM516 is a new model constructed in this study. The reference data in C and D were experimental data from published literature [39,48,49].

succinate synthesis pathway in *i*ZM4_478 may not be correct.

To confirm that genes involved in the complicated succinate biosynthesis pathway in *i*ZM516 were truly expressed *in vivo*, the transcriptional expression levels of these genes under different conditions were analyzed using the one-stop database ZymOmics (http://zymomics.cn/), which suggested that these genes were indeed expressed with low to middle level under different conditions (Fig. 4B). Meanwhile, compared with natural and engineered succinate producers, the pathway used for succinate synthesis in wild-type *Z. mobilis* is complicated and inefficient, and metabolic engineering strategies are needed to introduce heterologous pathways into *Z. mobilis* for efficient succinate biosynthesis.

3.5. Simulation of succinate production at high yield in Z. mobilis using iZM516

To the best of our knowledge, the maximum yield of succinate synthesis pathway was from the reductive branch of the TCA cycle (redTCA) with 1.71 mol/mol theoretical yield, which was from Pep to Oaa, then followed by the malate reduced pathway [53]. Based on above analyses, the related genes (*mdh* and *frd*) and reactions (rxn00248 and rxn00284) within redTCA were introduced into *i*ZM516 to explore the optimal succinate production pathway. Meanwhile, other genes from literature for succinate production were also introduced into *i*ZM516, such as *pck*, *sucAB* in oxTCA and *pfk* in Embden-Meyerhof-Parnas (EMP) pathway to enhance the precursor supply. The simulation results suggested that the introduction of only one key gene into *Z. mobilis* cannot improve succinate production significantly (Fig. 5A), therefore the combination simulation strategies were conducted (Fig. 5A).

In the succinate synthesis pathway, two important precursors are Pep and pyruvate. Therefore, enhancing the fluxes from Pep or pyruvate to redTCA is an effective strategy to improve the succinate production. For example, the fluxes can be enhanced from Pep into redTCA by introducing Pck, Mdh combining with the downstream reaction of "Fum + NADH - > Succ + NAD^+" catalyzed by fumarate reductase (Frd). In this way, the yield of succinate was able to achieve 0.98 mol/mol (Fig. 5A), which can also be achieved with the same yield by introducing MaeA and Frd. When the redTCA and oxTCA pathways were combined to improve precursors in different strategies, the yield of succinate can be achieved to 1.14–1.18 mol/mol. However, the native ED pathway in *Z. mobilis* usually produces one mol Pep and two mol pyruvate from one mol glucose. Therefore, if the native ED pathway is used for succinate production, the key enzyme MaeA will not only compete NADH with ethanol generation pathway, but also fixes one mol CO_2 in each reaction. The simulation result exhibited that the succinate yield could reach 84% of theoretical yield to 1.68 mol/mol coupling with CO_2 fixation (Fig. 5A and B).

In other way, the succinate yield can be enhanced to 1.47 mol/mol with the combination of redTCA and oxTCA fluxes by supplying the precursor Pep using EMP pathway through the introduction of *pfk* gene. If CO_2 was supplied infinitely to meet the maximum CO_2 fixation by Pck, the yield can be further improved 15% up to 1.68 mol/mol (Fig. 5A and C), which was consisted with 83.3% from the redTCA and 16.7% from the oxTCA. Above simulation thus suggested that the strategy to combine redTCA and oxTCA with CO_2 fixation is effective for succinate production in *Z. mobilis*, either using ED pathway or EMP pathway. Since succinate production under anaerobic condition has economic advantages, the *in-silico* simulation using industrial microorganisms such as *Z. mobilis* can provide guidance on designing metabolic pathways and microbial cell factories for succinate production under anaerobic conditions.

3.6. Exploration of 1,4-butanediol biosynthesis strategy in Z. mobilis using iZM516

1,4-Butanediol (1,4-BDO) is another platform chemical used for numerous applications. There has no natural microorganisms for 1,4-BDO production, and it is majorly produced by recombinant

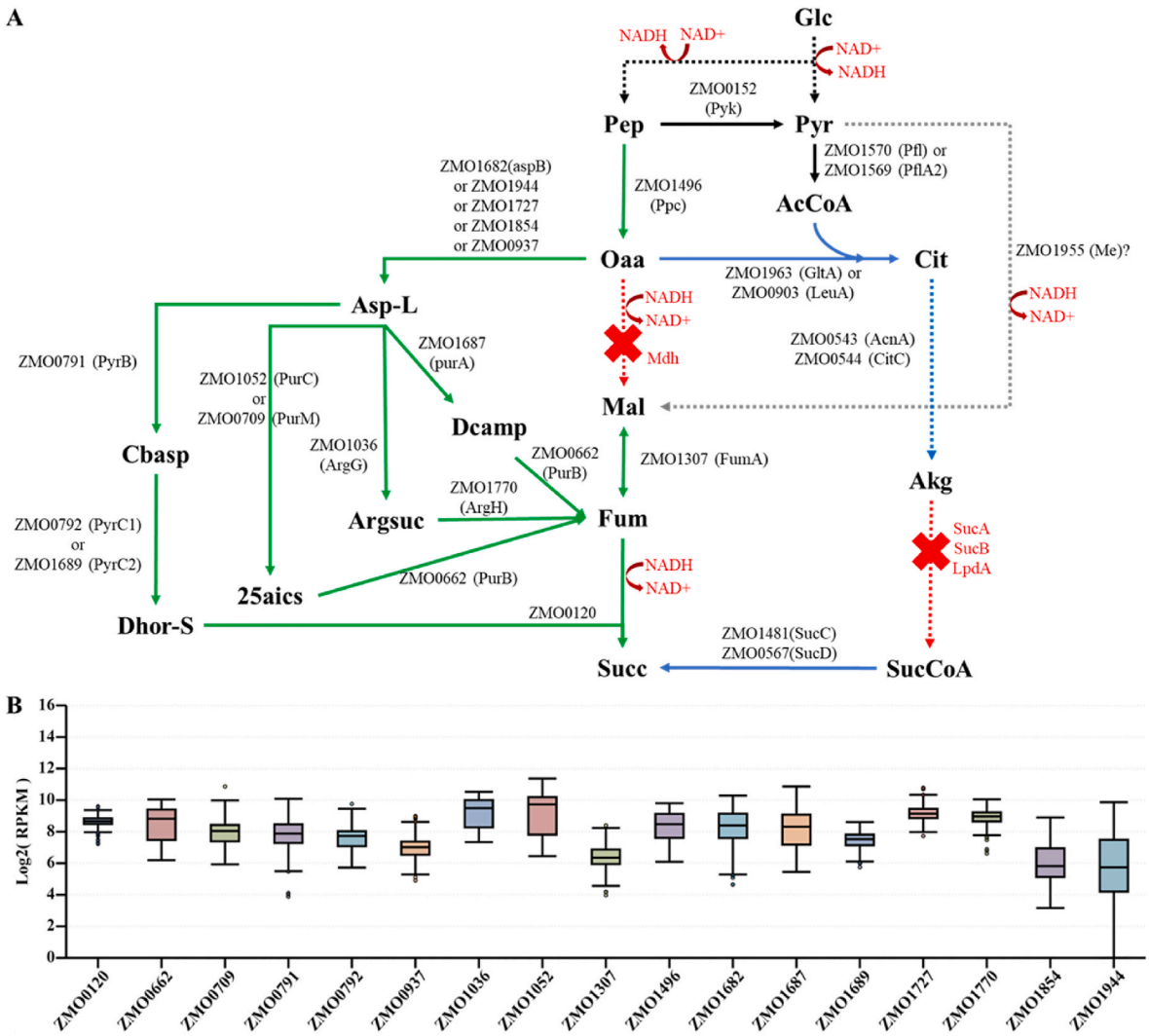

Fig. 4. The potential pathway of succinate generation in wild-type *Z. mobilis* (A), and the transcriptome expression box plot of genes in succinate synthesis pathway (B). The red cross lines represent the missing genes in the genome of *Z. mobilis*. The black and blue dot lines indicate there may have multiple reaction steps. The green lines represent the succinate synthetic pathway suggested by simulation of *i*ZM516. **25aics**: 5′-phosphoribosyl-4-(N-succinocarboxamide)-5-aminoimidazole, **AcCoA**: acetyl-CoA, **Akg**: 2-oxoglutarate (2-ketoglutaric acid), **Argsuc**: L-arginino-succinate, **Asp-L**: L-aspartate, **Cbasp**: N-carbamoyl-L-aspartate, **Cit**: citrate, **Dcamp**: adenylosuccinate, **Dhor-S**: (S)-dihydroorotate, **Fum**: fumarate, **Mal**: L-Malate, **Oaa**: oxaloacetate, **Pep**: phosphoenolpyruvate, **Pyr**: pyruvate, **Succ**: Succinate, **SucCoA**: succinyl-CoA.

microorganisms by introducing artificial biosynthesis pathways [54]. The pathway proposed by Kim et al. through biopathway prediction algorithms had high 1,4-BDO yield compared with other published pathways [54,55]. Since 1,4-BDO is the downstream product of succinate or Akg from TCA cycle, which was defined as BDO-succ (the precursor is from succinate) and BDO-akg (the precursor is from 2-oxoglutarate) pathway in this study, the production of 1,4-BDO was further simulated based on the succinate results using *i*ZM516 to help design and construct the metabolic pathways for 1,4-BDO production in *Z. mobilis*.

The simulation results suggested that the yield of 1,4-BDO was low if introducing either BDO-succ or BDO-akg 1,4-BDO production pathway only. The complicated biosynthesis pathway of succinate in wild-type *Z. mobilis* resulted in low yield of 1,4-BDO using BDO-succ pathway (Fig. 4A and 6). To optimize the production of 1,4-BDO, different combination strategies were tested using *i*ZM516 for efficient precursor supply or redox balance (Fig. 6). Through introducing Pck into BDO-akg pathway to enhance Oaa and energy supply, the 1,4-BDO yield was improved 88% compared with introducing BDO-akg pathway only. When combining Mdh and Frd as well as Pck or MaeA into the two pathways respectively, the yield was increased as expected because of the precursor enrichment, but the yield was limited to 0.54–0.56 mol (1,4-BDO)/mol (glucose). The modeling result demonstrated that the BDO-succ pathway consumes NADPH, while BDO-akg pathway produces NADPH (Fig. 6). Therefore, two pathways were combined with each route contributing 50% fluxes for redox balance during the simulation, the optimal yield can then be achieved to 0.79 mol (1,4-BDO)/mol (glucose) that is as high as the yield reported before [56]. It is worth noting that the optimal pathway to synthesize 1,4-BDO was not based on the highest succinate production pathway due to the imbalance of cofactor, energy, and biomass, which indicated that *in silico* simulation is beneficial before carrying out experiments.

3.7. Comparisons of succinate and 1,4-BDO production simulated with the models of Z. mobilis and E. coli

Since the model species *E. coli* is the most studied prokaryotic chassis cell for biochemical production and has been successfully engineered to produce succinate and 1,4-BDO, the complete GEM *i*ML1515 of *E. coli* [6] was used to compare the yields of succinate and 1,4-BDO with

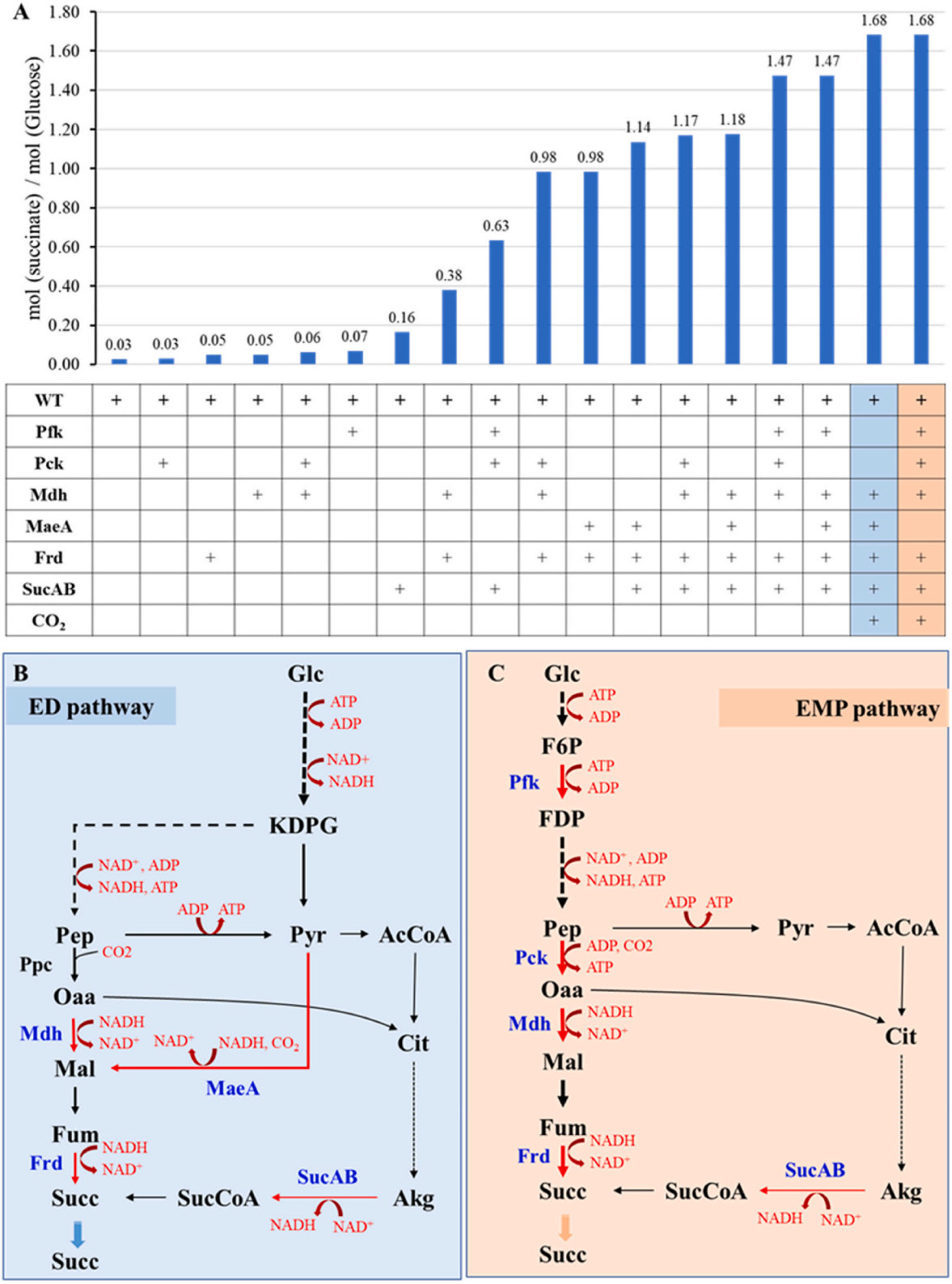

Fig. 5. Comparisons of different strategies for succinate production in *Z. mobilis* using the *in-silico* simulation (A) as well as the heterologous genes needed for succinate production through ED pathway (B) or EMP pathway (C). AcCoA: acetyl-CoA, **Akg**: 2-oxoglutarate (2-ketoglutaric acid), **Cit**: citrate, **F6P**: fructose-6-phosphate, **Frd**: fumarate reductase, **Fum**: fumarate, **Glc**: glucose, **KDPG**: 2-Keto-3-deoxy-6-phosphogluconate, **MaeA**: malate dehydrogenase, **Mal**: L-Malate, **Mdh**: malate dehydrogenase, **Oaa**: oxaloacetate, **Pep**: phosphoenolpyruvate, **Pyr**: pyruvate, **Pck**: PEP carboxykinase, **Pfk**: 6-phosphofructokinase, **SucAB**: α-ketoglutarate dehydrogenase complex, **Succ**: Succinate, **SucCoA**: succinyl-CoA. The blue fonts in B and C represent the enzyme catalyzing the reactions.

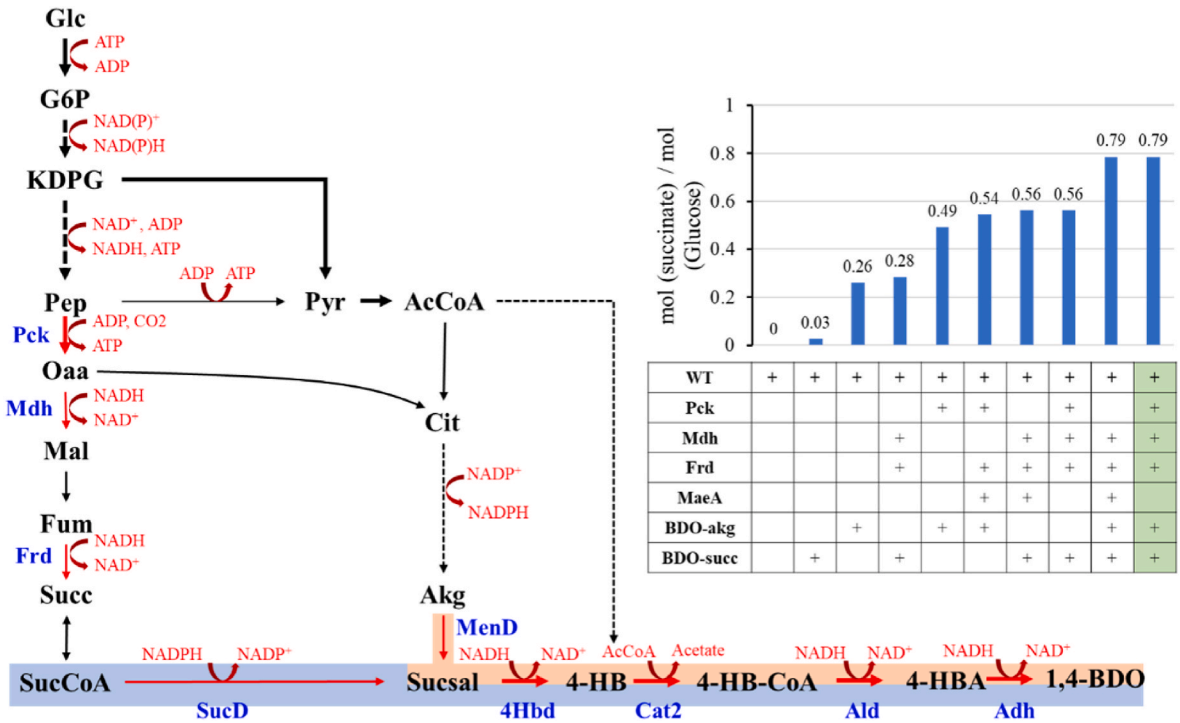

Fig. 6. The strategies for 1,4-BOD production in *Z. mobilis* based on *in silico* GEM simulation. 1,4-BDO: 1,4-butanediol, **4-HB**: 4-hydroxybutyrare, **4-HBA**: 4-hydroxybutyraldehyde, **4-HB-CoA**: 4-hydroxybutyryl-CoA, **AcCoA**: acetyl-CoA, **Akg**: 2-oxoglutarate (2-ketoglutaric acid), **Cit**: citrate, **Frd**: fumarate reductase, **Fum**: fumarate, **Glc**: glucose, **KDPG**: 2-Keto-3-deoxy-6-phosphogluconate, **Mal**: L-Malate, **Mdh**: malate dehydrogenase, **Oaa**: oxaloacetate, Pep: phosphoenolpyruvate, **Pck**: phosphoenolpyruvate carboxykinase, **Pyr**: pyruvate, **Succ**: succinate, **SucCoA**: succinyl-CoA, **SucD**: succinate semialdehyde dehydrogenase, **Sucsal**: succinate semialdehyde. The blue fonts in B and C represent the enzyme catalyzed the reaction.

Z. mobilis. While *E. coli* naturally harbors the succinate synthesis pathway, no heterologous gene was introduced into the model *i*ML1515. The simulation results suggested that the maximum yield of succinate can be achieved to 1.68 mol/mol with cell growth rate set as 0.1 h^{-1} under anaerobic condition, which is as high as the optimal yield in *Z. mobilis* (Table 3), and was higher than that of 1.5 mol/mol for the previous recombinant strain [57]. When the 1,4-BDO synthesis pathway was introduced into *i*ML1515, 0.99 mol/mol 1,4-BDO will be produced in *E. coli*, which was higher than that of 0.79 mol/mol in *Z. mobilis* (Table 3).

By comparing metabolic pathways, we found that the primary byproduct acetate was utilized in *E. coli*, which shed light on enhancing 1,4-BDO yield in *Z. mobilis*. Therefore, the pathway that recycling acetate to generate acetyl-CoA by ATP: acetate phosphotransferase (AckA) and acetyl-CoA: phosphate acetyltransferase (Pta) was introduced into *i*ZM516. As a result, the yield of 1,4-BDO can be increased to 1.07 mol/mol in *Z. mobilis* (Table 3), which was higher than that of *E. coli* due to the lower ATP maintenance requirement of *Z. mobilis*. It should be noted that the reaction of converting acetate to acetyl-phosphate by AckA was an ATP consuming reaction. Thus, it is necessary to complete EMP pathway in *Z. mobilis* to supply more ATP, which was confirmed by simulation using *i*ZM516.

Although the *E. coli* was successfully engineered to produce succinate [57] and 1,4-BDO [55], there still has the space to enhance the yield based on the simulation. Compared with *E. coli*, *Z. mobilis* has the same yield of succinate and higher optimal yield of 1,4-BDO when acetate recycle was applied under anaerobic condition. Since *Z. mobilis* possesses industrial characteristics such as anaerobic fermentation at a broad range of pH and temperature conditions, few byproducts, free of phage infection, and robustness against lignocellulosic inhibitors [40], it will be an excellent chassis cell to be developed as microbial cell factories for the industrial-scale production of lignocellulosic biofuels and biochemicals.

Meanwhile, our results also exhibited that the *in silico* modeling and analysis is an effective approach to evaluate the design of metabolic pathways and microbial cell factories before experimentation, which is not only important for model microorganisms such as *E. coli* with tremendous amount of experimental data and comprehensive databases, but also vital for those non-model microorganisms with specific industrial characteristics such as *Z. mobilis* in this study [58]. Therefore, high-quality GEMs and comprehensive strain specific databases are necessary to reduce the time and cost associated with the classical trial-and-error research approach, and lay the foundation to facilitate the construction of digital cells in the future.

Table 3
Comparisons of succinate and 1,4-butanediol (1,4-BDO) production using genome-scale metabolic models of *Z. mobilis* and *E. coli*.

Model	Chassis cell	Succinate (mol/mol)	1,4-BDO (Acetate not recycle) (mol/mol)	1,4-BDO (Acetate recycle) (mol/mol)
*i*ZM516	*Z. mobilis*	1.68	0.79	1.07
*i*ML1515	*E. coli*	1.68	0.79	0.99

4. Conclusion

In this work, a high-quality GEM *i*ZM516 of *Z. mobilis* ZM4 was constructed based on the improved genomic information, experimental datasets of Biolog Phenotype Microarrays, databases, and literature reports. The model *i*ZM516 contains 1389 reactions, 1437 metabolites, 516 genes, and 3 cell compartments, and has the highest MEMOTE evaluation score 91% among all published models of *Z. mobilis*. Based on *i*ZM516, the native succinate synthesis pathway in *Z. mobilis* was examined and proposed, and the potential of *Z. mobilis* to produce succinate and 1,4-BDO with high yield under anaerobic condition was then evaluated using *i*ZM516. The modeling results suggested that 1.68 mol/

mol succinate and 1.07 mol/mol 1,4-BDO can be achieved through metabolic engineering in *Z. mobilis*. Therefore, this high-quality genome-scale metabolic model *i*ZM516 of *Z. mobilis* developed in this study not only offers a new tool to expend the product spectrum using *Z. mobilis* as the chassis cell, but also provides a guidance on developing high-quality GEMs to facilitate the rational design of metabolic pathways and microbial cell factories using non-model industrial microorganisms. This study provided a theoretical analysis for different products, and the experimental validation is needed in the future work.

Funding

This work was supported by the National Key Technology Research and Development Program of China (2018YFA0900300 and 2022YFA0911800), the National Natural Science Foundation of China (21978071 and U1932141), the Key Science and Technology Innovation Project of Hubei Province (2021BAD001), 2022 Joint Projects between Chinese and CEEC's Universities (202004), the Leading Innovative and Entrepreneur Team Introduction Program of Zhejiang Province (2018R01014), and the Innovation Base for Introducing Talents of Discipline of Hubei Province (2019BJH021). Funding was also supported by State Key Laboratory of Biocatalysis and Enzyme Engineering.

CRediT authorship contribution statement

Yalun Wu: Data curation, Visualization, Writing – original draft. **Qianqian Yuan:** Data curation, Visualization, Writing – original draft. **Yongfu Yang:** Experimentation, Data curation, Visualization, Writing – original draft. **Defei Liu:** Methodology, and, Experimentation. **Shihui Yang:** Conceptualization, Funding acquisition, Supervision, Writing – review & editing. **Hongwu Ma:** Conceptualization, Funding acquisition, Supervision, Writing – review & editing, All authors have read and approved the final manuscript.

Declaration of competing interest

All authors declare that they have no conflicts of interest.

Appendix A. Supplementary data

Supplementary data to this article can be found online at https://doi.org/10.1016/j.synbio.2023.07.001.

References

[1] Yilmaz S, Nyerges A, van der Oost J, Church GM, Claassens NJ. Towards next-generation cell factories by rational genome-scale engineering. Nat Catal 2022;5(9):751–65.
[2] Fang X, Lloyd CJ, Palsson BO. Reconstructing organisms in silico: genome-scale models and their emerging applications. Nat Rev Microbiol 2020;18(12):731–43.
[3] Gu CD, Kim GB, Kim WJ, Kim HU, Lee SY. Current status and applications of genome-scale metabolic models. Genome Biol 2019;20:121.
[4] Chen Y, Li F, Nielsen J. Genome-scale modeling of yeast metabolism: retrospectives and perspectives. FEMS Yeast Res 2022;22(1):1–9.
[5] Edwards JS, Palsson BO. The *Escherichia coli* MG1655 in silico metabolic genotype: its definition, characteristics, and capabilities. Proc Natl Acad Sci USA 2000;97(10):5528–33.
[6] Monk JM, Lloyd CJ, Brunk E, Mih N, Sastry A, King Z, Takeuchi R, Nomura W, Zhang Z, Mori H, et al. *i*ML1515, a knowledgebase that computes *Escherichia coli* traits. Nat Biotechnol 2017;35(10):904–8.
[7] Yang X, Mao Z, Zhao X, Wang R, Zhang P, Cai J, Xue C, Ma H. Integrating thermodynamic and enzymatic constraints into genome-scale metabolic models. Metab Eng 2021:133–44.
[8] Li F, Yuan L, Lu H, Li G, Chen Y, Engqvist MKM, Kerkhoven EJ, Nielsen J. Deep learning-based kcat prediction enables improved enzyme-constrained model reconstruction. Nat Catal 2022;5:662–72.
[9] Xia J, Yang YF, Liu CG, Yang SY, Bai FW. Engineering *Zymomonas mobilis* for robust cellulosic ethanol production. Trends Biotechnol 2019;37(9):960–72.
[10] Wang X, He Q, Yang Y, Wang J, Haning K, Hu Y, Wu B, He M, Zhang Y, Bao J, et al. Advances and prospects in metabolic engineering of *Zymomonas mobilis*. Metab Eng 2018;50:57–73.
[11] Yan Z, Zhang J, Bao J. Increasing cellulosic ethanol production by enhancing phenolic tolerance of *Zymomonas mobilis* in adaptive evolution. Bioresour Technol 2021;329:124926.
[12] Geng B, Liu S, Chen Y, Wu Y, Wang Y, Zhou X, Li H, Li M, Yang S. A plasmid-free Zymomonas mobilis mutant strain reducing reactive oxygen species for efficient bioethanol production using industrial effluent of xylose mother liquor. Front Bioeng Biotechnol 2022;10:1110513.
[13] Li Y, Wang Y, Wang R, Yan X, Wang J, Wang X, Chen S, Bai F, He Q, Yang S. Metabolic engineering of *Zymomonas mobilis* for continuous co-production of bioethanol and poly-3-hydroxybutyrate (PHB). Green Chem 2022;24(6):2588–601.
[14] Lawford HG, Rousseau JD. Steady-state measurements of lactic acid production in a wild-type and a putative D-lactic acid dehydrogenase-negative mutant of *Zymomonas mobilis*: influence of glycolytic flux. Appl Biochem Biotechnol 2002;98–100:215–28.
[15] Liu Y, Ghosh IN, Martien J, Zhang Y, Amador-Noguez D, Landick R. Regulated redirection of central carbon flux enhances anaerobic production of bioproducts in *Zymomonas mobilis*. Metab Eng 2020;61:261–74.
[16] Yang S, Mohagheghi A, Franden MA, Chou YC, Chen X, Dowe N, Himmel ME, Zhang M. Metabolic engineering of *Zymomonas mobilis* for 2,3-butanediol production from lignocellulosic biomass sugars. Biotechnol Biofuels 2016;9(1):189.
[17] Folle AB, Baschera VM, Vivan LT, Carra S, Polidoro TA, Malvessi E, da Silveira MM. Assessment of different systems for the production of aldonic acids and sorbitol by calcium alginate-immobilized *Zymomonas mobilis* cells. Bioproc Biosyst Eng 2018;41(2):185–94.
[18] Kalnenieks U, Balodite E, Strahler S, Strazdina I, Rex J, Pentjuss A, Fuchino K, Bruheim P, Rutkis R, Pappas KM, et al. Improvement of acetaldehyde production in *Zymomonas mobilis* by engineering of its aerobic metabolism. Front Microbiol 2019;10:2533.
[19] Qiu M, Shen W, Yan X, He Q, Cai D, Chen S, Wei H, Knoshaug EP, Zhang M, Himmel ME, et al. Metabolic engineering of *Zymomonas mobilis* for anaerobic isobutanol production. Biotechnol Biofuels 2020;13:15.
[20] Lee KY, Park JM, Kim TY, Yun H, Lee SY. The genome-scale metabolic network analysis of *Zymomonas mobilis* ZM4 explains physiological features and suggests ethanol and succinic acid production strategies. Microb Cell Factories 2010;9:94.
[21] Widiastuti H, Kim JY, Selvarasu S, Karimi IA, Kim H, Seo JS, Lee DY. Genome-scale modeling and in silico analysis of ethanologenic bacteria *Zymomonas mobilis*. Biotechnol Bioeng 2011;108(3):655–65.
[22] Goodman AE, Rogers PL, Skotnicki ML. Minimal medium for isolation of auxotrophic *Zymomonas mutants*. Appl Environ Microbiol 1982;44(2):496–8.
[23] Nouri H, Fouladiha H, Moghimi H, Marashi SA. A reconciliation of genome-scale metabolic network model of *Zymomonas mobilis* ZM4. Sci Rep 2020;10(1):7782.
[24] Seo JS, Chong H, Park HS, Yoon KO, Jung C, Kim JJ, Hong JH, Kim H, Kim JH, Kil JI, et al. The genome sequence of the ethanologenic bacterium *Zymomonas mobilis* ZM4. Nat Biotechnol 2005;23(1):63–8.
[25] Yang S, Pappas KM, Hauser LJ, Land ML, Chen GL, Hurst GB, Pan C, Kouvelis VN, Typas MA, Pelletier DA, et al. Improved genome annotation for *Zymomonas mobilis*. Nat Biotechnol 2009;27(10):893–4.
[26] Yang S, Vera JM, Grass J, Savvakis G, Moskvin OV, Yang Y, McIlwain SJ, Lyu Y, Zinonos I, Hebert AS, et al. Complete genome sequence and the expression pattern of plasmids of the model ethanologen *Zymomonas mobilis* ZM4 and its xylose-utilizing derivatives 8b and 2032. Biotechnol Biofuels 2018;11:125.
[27] Brettin T, Davis JJ, Disz T, Edwards RA, Gerdes S, Olsen GJ, Olson R, Overbeek R, Parrello B, Pusch GD, et al. RASTtk: a modular and extensible implementation of the RAST algorithm for building custom annotation pipelines and annotating batches of genomes. Sci Rep 2015;5:8365.
[28] Sayers EW, Beck J, Brister JR, Bolton EE, Canese K, Comeau DC, Funk K, Ketter A, Kim S, Kimchi A, et al. Database resources of the National Center for biotechnology information. Nucleic Acids Res 2020;48(D1):D9–16.
[29] Caspi R, Billington R, Keseler IM, Kothari A, Krummenacker M, Midford PE, Ong WK, Paley S, Subhraveti P, Karp PD. The MetaCyc database of metabolic pathways and enzymes - a 2019 update. Nucleic Acids Res 2020;48(D1):D445–53.
[30] Norsigian CJ, Pusarla N, McConn JL, Yurkovich JT, Drager A, Palsson BO, King Z. BiGG Models 2020: multi-strain genome-scale models and expansion across the phylogenetic tree. Nucleic Acids Res 2020;48(D1):D402–6.
[31] Chang A, Jeske L, Ulbrich S, Hofmann J, Koblitz J, Schomburg I, Neumann-Schaal M, Jahn D, Schomburg D. BRENDA, the ELIXIR core data resource in 2021: new developments and updates. Nucleic Acids Res 2021;49(D1):D498–508.
[32] Beber ME, Gollub MG, Mozaffari D, Shebek KM, Flamholz AI, Milo R, Noor E. eQuilibrator 3.0: a database solution for thermodynamic constant estimation. Nucleic Acids Res 2022;50(D1):D603–9.
[33] Brenac L, Baidoo EEK, Keasling JD, Budin I. Distinct functional roles for hopanoid composition in the chemical tolerance of *Zymomonas mobilis*. Mol Microbiol 2019;112(5):1564–75.
[34] Luo J, Yuan Q, Mao Y, Wei F, Zhao J, Yu W, Kong S, Guo Y, Cai J, Liao X, et al. Reconstruction of a genome-scale metabolic network for *Shewanella oneidensis* MR-1 and analysis of its metabolic potential for bioelectrochemical systems. Front Bioeng Biotechnol 2022;10:913077.
[35] Ma H, Zeng AP. Reconstruction of metabolic networks from genome data and analysis of their global structure for various organisms. Bioinformatics 2003;19(2):270–7.
[36] Bochner B, Gomez V, Ziman M, Yang S, Brown SD. Phenotype microarray profiling of *Zymomonas mobilis* ZM4. Appl Biochem Biotechnol 2010;161(1–8):116–23.
[37] Ebrahim A, Lerman JA, Palsson BO, Hyduke DR. COBRApy: COnstraints-based reconstruction and analysis for Python. BMC Syst Biol 2013;7:74.

[38] Lieven C, Beber ME, Olivier BG, Bergmann FT, Ataman M, Babaei P, Bartell JA, Blank LM, Chauhan S, Correia K, et al. MEMOTE for standardized genome-scale metabolic model testing. Nat Biotechnol 2020;38(3):272–6.
[39] Jacobson TB, Adamczyk PA, Stevenson DM, Regner M, Ralph J, Reed JL, Amador-Noguez D. ^{2}H and ^{13}C metabolic flux analysis elucidates in vivo thermodynamics of the ED pathway in *Zymomonas mobilis*. Metab Eng 2019;54:301–16.
[40] Wang X, He QN, Yang YF, Wang JW, Haning K, Hu Y, Wu B, He MX, Zhang YP, Bao J, et al. Advances and prospects in metabolic engineering of *Zymomonas mobilis*. Metab Eng 2018;50:57–73.
[41] Kalnenieks U, Balodite E, Rutkis R. Metabolic engineering of bacterial respiration: high vs. low P/O and the case of *Zymomonas mobilis*. Front Bioeng Biotechnol 2019;7:327.
[42] Kalnenieks U, Galinina N, Strazdina I, Kravale Z, Pickford JL, Rutkis R, Poole RK. NADH dehydrogenase deficiency results in low respiration rate and improved aerobic growth of *Zymomonas mobilis*. Microbiology (Read) 2008;154(Pt 3):989–94.
[43] Martien JI, Hebert AS, Stevenson DM, Regner MR, Khana DB, Coon JJ, Amador-Noguez D. Systems-level analysis of oxygen exposure in *Zymomonas mobilis*: implications for isoprenoid production. mSystems 2019;4(1):1–23.
[44] Ong WK, Courtney DK, Pan S, Andrade RB, Kiley PJ, Pfleger BF, Reed JL. Model-driven analysis of mutant fitness experiments improves genome-scale metabolic models of *Zymomonas mobilis* ZM4. PLoS Comput Biol 2020;16(8):e1008137.
[45] Felczak MM, TerAvest MA. *Zymomonas mobilis* ZM4 utilizes an NADP(+)-dependent acetaldehyde dehydrogenase to produce acetate. J Bacteriol 2022:e0056321.
[46] Motamedian E, Saeidi M, Shojaosadati SA. Reconstruction of a charge balanced genome-scale metabolic model to study the energy-uncoupled growth of *Zymomonas mobilis* ZM1. Mol Biosyst 2016;12(4):1241–9.
[47] Yan X, Wang X, Yang Y, Wang Z, Zhang H, Li Y, He Q, Li M, Yang S. Cysteine supplementation enhanced inhibitor tolerance of *Zymomonas mobilis* for economic lignocellulosic bioethanol production. Bioresour Technol 2022:126878.
[48] Fuhrer T, Fischer E, Sauer U. Experimental identification and quantification of glucose metabolism in seven bacterial species. J Bacteriol 2005;187(5):1581–90.
[49] Kremer TA, LaSarre B, Posto AL, McKinlay JB. N_2 gas is an effective fertilizer for bioethanol production by *Zymomonas mobilis*. Proc Natl Acad Sci U S A 2015;112(7):2222–6.
[50] Shui Z, Wang J, Qin H, Wu B, Tan F, Mingxiong H. Construction and preliminary fermentation of succinate-producing recombinant ethanologenic *Zymomonas mobilis*. Chin J Appl Environ Biol 2015;21:657–64.
[51] Swings J, De Ley J. The biology of *Zymomonas*. Bacteriol Rev 1977;41(1):1–46.
[52] Widiastuti H, Lee N-R, Karimi I, Lee D-Y. Genome-scale in silico analysis for enhanced production of succinic acid in *Zymomonas mobilis*. Processes 2018;6(4):30.
[53] Thoma F, Schulze C, Gutierrez-Coto C, Hadrich M, Huber J, Gunkel C, Thoma R, Blombach B. Metabolic engineering of *Vibrio natriegens* for anaerobic succinate production. Microb Biotechnol 2022;15(6):1671–84.
[54] Cheng J, Li J, Zheng L. Achievements and perspectives in 1,4-butanediol production from engineered microorganisms. J Agric Food Chem 2021;69(36):10480–5.
[55] Yim H, Haselbeck R, Niu W, Pujol-Baxley C, Burgard A, Boldt J, Khandurina J, Trawick JD, Osterhout RE, Stephen R, et al. Metabolic engineering of *Escherichia coli* for direct production of 1,4-butanediol. Nat Chem Biol 2011;7(7):445–52.
[56] Burgard A, Burk MJ, Osterhout R, Van Dien S, Yim H. Development of a commercial scale process for production of 1,4-butanediol from sugar. Curr Opin Biotechnol 2016;42:118–25.
[57] Zhu X, Tan Z, Xu H, Chen J, Tang J, Zhang X. Metabolic evolution of two reducing equivalent-conserving pathways for high-yield succinate production in *Escherichia coli*. Metab Eng 2014;24:87–96.
[58] Helmy M, Smith D, Selvarajoo K. Systems biology approaches integrated with artificial intelligence for optimized metabolic engineering. Metab Eng Commun 2020;11:e00149.